Confinement-dependent localization of diffusing aggregates in cellular geometries

Mahdi Rezaei Keramati,[1,2] Vaihbav Wasnik,[1] Liyan Ping,[3] Dibyendu Das,[4] and Eldon Emberly[1,*]
[1]*Physics Department, Simon Fraser University, Burnaby, BC, V5A 1S6, Canada*
[2]*Department of Theoretical Physics, University of Tabriz, Tabriz, Iran*
[3]*Rowland Institute, Harvard University, Cambridge, Massachusetts, USA*
[4]*Department of Physics, Indian Institute of Technology, Bombay, Powai, Mumbai, India*
(Received 7 July 2014; published 20 January 2015)

Confinement has a strong influence on diffusing nano-sized clusters. In particular, biomolecular aggregates within the shell-like confining space of a bacterial cell have been shown to display a variety of localization patterns, from being midcell to the poles. How does the confining space determine where the aggregate will localize? Here, using Monte Carlo simulations we have calculated the equilibrium spatial distribution of fixed-sized clusters diffusing in spherocylindrical shells. We find that localization to the poles depends strongly on shell thickness and the size of the cluster. Compared to being at midcell, polar clusters can be more bent and hence have higher energy, but they also can have a greater number of defects and hence have more entropy. Under certain conditions this can lead to polar clusters having a lower free energy than at midcell, favoring localization to the poles. Our findings suggest possible localization selection mechanisms within shell-like geometries that can arise purely from cluster confinement.

DOI: 10.1103/PhysRevE.91.012705 PACS number(s): 87.15.bk, 68.35.Dv, 68.43.Jk, 87.15.Vv

I. INTRODUCTION

A variety of examples in nature show that interacting particles in confined geometries can display a variety of spatial organization, from the uniform arrangement of clusters on the surface of a cell [1,2] to the polar localization of proteins within the cytoplasmic space [3–8]. Modeling efforts showed that curvature effects due to confinement to the membrane [9] or the crowding of the bacterial DNA are potential mechanisms leading to the observed localization [7,10–12]. As another example, it has long been known that vital dyes show polar localization in bacteria, and recent experimental work has shown that they are confined to the shell-shaped space known as the periplasm [13]. In this case, unlike localization that was due to interactions with the membrane or the bacterial DNA, modeling showed that the shell-like confining space of the periplasm could be a sufficient localizing mechanism [13]. Support for the importance of such confinement effects has been found in colloidal systems both experimentally [14–19] and theoretically [20–22]. In particular, it was found that cluster shape [23] determines the type of motion it can perform and this strongly depends on the geometry of the confining space. For a spherocylindrical shell, such as the periplasmic space of a bacteria, how does the confining space alter the shape of an aggregate as it moves? and does this play any role in its localization?

Recent simulations have explored the behavior of aggregating particles that diffuse within confining spaces [7,10–13,21]. In these models, particles have attractive interactions that cause them to cluster, and then the cluster is free to diffuse within the space bounded by hard walls. The motion of the center of mass is determined by the collective behavior of all the particles which is influenced by the local confining space. A minimal model was used to explore cluster localization in a confining space like the periplasm and showed that polar localization could be favored which depended on the thickness of the shell, but was confounded by also depending on the cluster's rate of growth [13].

In this paper we explore the equilibrium localization of fixed-size clusters in a spherocylindrical confining shell [see Fig. 1(a)]. We find that localization to either the poles or the midcell region can be favored at particular shell thicknesses. By analyzing the energetics and entropy of the system we show that localization is determined by the spatially dependent packing of its constituents.

II. SIMULATING CLUSTERS IN A CONFINED SHELL GEOMETRY

We consider N diffusing particles within a confining volume that consists of a cylindrical shell capped with two hemispherical shells [see Fig. 1(a)]. Such a geometry is found in the periplasmic space, or potentially the cytoplasmic space between the nucleoid and the inner membrane of rod-shaped bacteria. We consider the cylindrical region to have length L. The shell has inner and outer radii, R_I and R_O, giving the thickness of the shell to be $h = R_O - R_I$. In what follows we will consider both two-dimensional (2D) and three-dimensional (3D) shells.

The diffusing particles have diameter σ and have an isotropic attractive interaction between them given by a 12-6 Lennard-Jones potential. The interaction energy between particle i and j is

$$E_{ij} = \epsilon \left[\left(\frac{\sigma}{r_{ij}} \right)^{12} - \left(\frac{\sigma}{r_{ij}} \right)^{6} \right], \tag{1}$$

where ϵ is the strength of the interaction and r_{ij} is the distance between the two particles.

In a given simulation, N particles are added at random locations within the confining shell. We use a Metropolis Monte Carlo (MC) method to track the motion and aggregation of the cluster. Each MC sweep consists of moving all N particles where each move is in a random direction in three dimensions

*Corresponding author: eemberly@sfu.ca

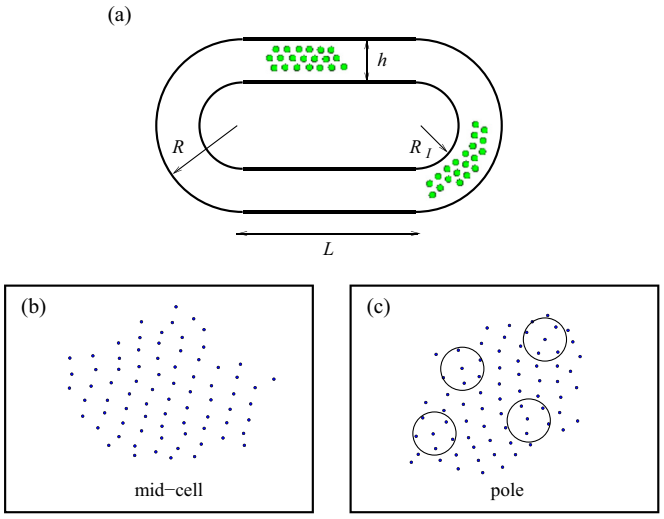

FIG. 1. (Color online) (a) Schematic of a cluster of N attractive particles diffusing in thin shell with thickness h. The shell geometry is a cylindrical shell capped with two hemispheres. The cylindrical region has a length L, the inner boundary has radius R_I, and the outer one radius R. The thickness of the shell is given by $h = R - R_I$. In all simulations we consider the aspect ratio to be $(2R + L)/2R = 2$. Shown is a cluster positioned at two locations: the midcell region and at one of the poles (for $N = 20$ from a 2D simulation). (b) A cluster with $N = 80$ at midcell for $h/\sigma = 1.25$ showing a highly regular hexagonal close packed structure. (c) A polar cluster with $N = 80$ for the same shell thickness $h/\sigma = 1.25$ showing the existence of defects (open circles) that reduce the number of nearest neighbors to fewer than six.

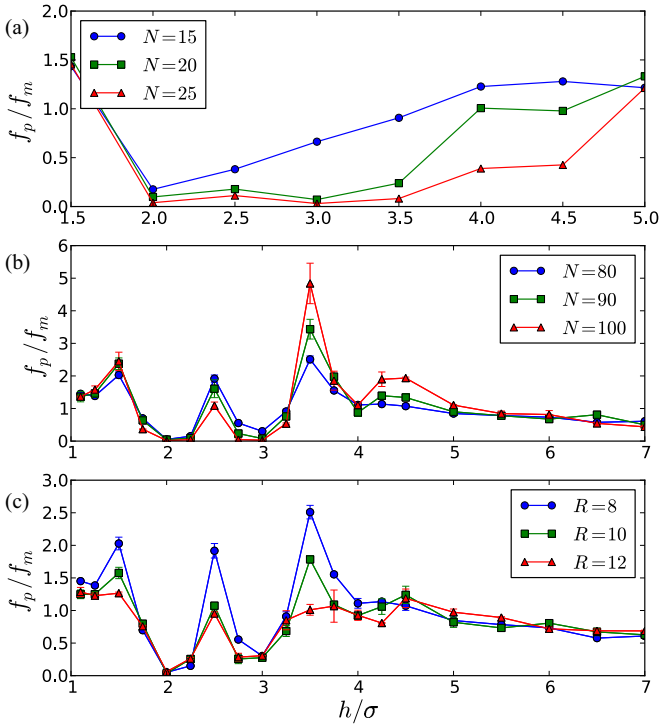

FIG. 2. (Color online) Calculated fractional residency as a function of shell thickness, h/σ. (a) Dependence of fractional residency on the cluster size, N, for a 2D shell geometry with $R = 8\sigma$ and $L = 16\sigma$. (b) Dependence on cluster size N for a 3D shell, with $R = 8\sigma$ and $L = 16\sigma$. (c) Effect of shell curvature (changing the outer radius) on fractional residency for a fixed-size cluster with $N = 80$ in 3D shells. (Error bars were estimated by halving the number of samples and calculating the change in f_p/f_m.)

(or two dimensions) with a maximum step size of equal to 0.1 σ. A move is accepted or rejected based on the Boltzmann weight that depends on the change in total energy [evaluated by summing over all pairwise interactions using Eq. (1)]. The walls of the confining shell are treated as hard barriers, and any move that takes a particle outside the shell is rejected.

The particle interaction energy is set at a value of $\epsilon = 3k_BT$ to ensure that on average all N particles reside in a single cluster, as this is well below the liquid-gas transition for a Lennard-Jones system. Each simulation begins with a cluster formation step where particles are added one by one every 10 000 sweeps. We find that this procedure is sufficient to generate a single cluster containing all N particles. After the cluster formation step, we typically carry out >4 billion sweeps and sample the configuration every 25 000 sweeps. This amount of sampling leads to a cluster traversing the shell length, 100s to 1000s of times. At each sample, the location of the center of mass (CoM) of the cluster is calculated. We determine which particles are in the cluster using an equivalence class algorithm [24] with a cutoff distance of $r_{\text{cut}} = 2.5\sigma$, which is the cutoff distance on the Lennard-Jones potential. The total binding energy of the cluster of particles is also calculated at every sample step.

III. DEPENDENCE OF CLUSTER LOCALIZATION ON CONFINEMENT

For a cluster consisting of a fixed number of particles N, we use our MC method above to generate the equilibrium distribution of its CoM coordinate, x, along the length of the spherocylindrical shell. Over the course of a simulation the cluster diffuses within the restricted volume. In order to characterize the effect of confinement, the ratio of the probability of being at the poles to the midcell is calculated. This fractional residency is given by $f_p/f_m = n_p/n_m$, where n_p is the number of samples when the CoM is in one of the polar hemispheres ($|x| > L/2$) and n_m is number of times it is in the central cylindrical shell ($|x| \leqslant L/2$).

In Fig. 2 we plot the fractional residency, f_p/f_m, as a function of the shell thickness scaled by the particle size, h/σ, under various conditions. Shown in Fig. 2(a) are the results for clusters of different sizes diffusing in a 2D shell. For very thin shells that admit just a single row of particles, the fractional residency is near unity. As the thickness of the shell increases, residency at the poles drops to near zero, and then when h/σ becomes large enough to admit a near circular cluster, the fractional residency again returns to being near unity. Figures 2(b) and 2(c) show the results for a cluster diffusing in a 3D shell where much more complex behavior emerges. Interestingly, the system alternates between having the cluster being strongly favored at the poles ($f_p/f_m > 1$) for half integer values of h/σ, to being localized at the midcell ($f_p/f_m < 1$) at integer values. At larger shell thicknesses the fraction of time spent at the midcell compared to the pole is limited to the value expected for a free spherical cluster

diffusing in the confined space, namely, the ratio of the sizes of the two regions (the same for 2D shells). We now discuss the dependency of the fractional residency f_p/f_m on other factors such as cluster size and shell curvature.

In Figs. 2(a) and 2(b) the fractional residency is shown for different values of N inside a shell whose outer boundary $R_O = R$ is fixed. Smaller clusters [(a) $N = 15$ or (b) $N = 80$] will be able to fit as a (circular) spherical cluster within the shell at smaller values of h/σ, which explains why the fractional residency tends to the free spherical cluster limit sooner. In 3D shells, as N increases, the effect of confinement continues to larger values of h/σ with a new peak emerging at $h/\sigma \approx 4.5$. Interestingly the polar localization decreases with N at $h/\sigma \approx 2.5$ but increases with N at $h/\sigma \approx 3.5$.

The effect of changing the shell's curvature is shown in Fig. 2(c) for 3D shells. Here N was fixed, but the outer radius was changed. Peaks in the fractional residency still occur at half integer values of h/σ, but the effect is less pronounced as the shell curvature decreases (i.e., R increases). Clusters at the pole experience additional bending compared to those at midcell, and decreasing the curvature of the cellular geometry reduces the energy difference between the two locations, thereby changing the fractional residency. We now examine the role of how confinement influences the energy and entropy of a cluster and the resulting effect on the fractional residency.

IV. ROLE OF ENERGY AND ENTROPY IN LOCALIZATION

The results from the previous section showed that the thickness of the shell can favor a cluster to reside at either the pole or the midcell in 3D shells, but not in two dimensions where the midcell was always preferred. At equilibrium, the fractional residency will depend only on the relative size of the polar to midcell regions as well as potentially any free energy difference between them. Our simulations show that for the sizes of clusters studied, confinement restricts the CoM motion to a surface that lies midway between the inner and outer radii of the shell. If the free energy difference between the pole and midcell were zero, then the fractional residency would simply go as the ratio of the surface area (or arc length in two dimensions) at the poles, A_p, to that at midcell, A_m. Given that the spherocylindrical surface on which the CoM travels has a radius $\bar{R} = R - h/2$, where R is the outer radius, this gives the ratio of areas to be $A_p/A_m = 2(R - h/2)/L$. In all of our simulations we have used $L = 2R$, so $A_p/A_m = 1 - h/2R$, which ranges from 1 to 1/2 when h goes from 0 to R. [For 2D shells, with $L = 2R$, the ratio of arc lengths is $A_p/A_m = (\pi/2)(1 - h/2R)$, which limits to $A_p/A_m = \pi/2$ as $h \to 0$.] At large values of h/σ where clusters are spherical and have little to no free energy difference between the pole and midcell, we see that f_p/f_m does indeed limit to 1/2 in 3D shells [see Figs. 2(b) and 2(c)].

For thinner shells, where the cluster is no longer spherical, f_p/f_m departs from the above limit of the ratio of the sizes of the polar to midcell regions, and this results from a free energy difference between the pole and midcell. To aid our analysis, we assume that as the cluster diffuses at either the pole (p) or midcell (m), it can be characterized by an average free energy, G_p or G_m which is roughly constant over the respective region. This average free energy for a cluster at $\mu = \{p,m\}$, can be written as $G_\mu = E_\mu - S_\mu$ where E_μ is the average cluster binding energy, and S_μ is the associated cluster entropy (using $\beta = 1/k_BT = 1$). The entropy of the cluster can be written as $S_\mu = \log(w_\mu)$ where w_μ is the number of cluster configurations, which may differ between the poles and midcell. At equilibrium, the fractional residency can then be written as

$$\frac{f_p}{f_m} = \frac{A_p}{A_m} e^{-(G_p - G_m)} = \frac{A_p}{A_m} e^{-(E_p - E_m)} \frac{w_p}{w_m}. \quad (2)$$

We first look at how the variation in the cluster's binding energy affects localization.

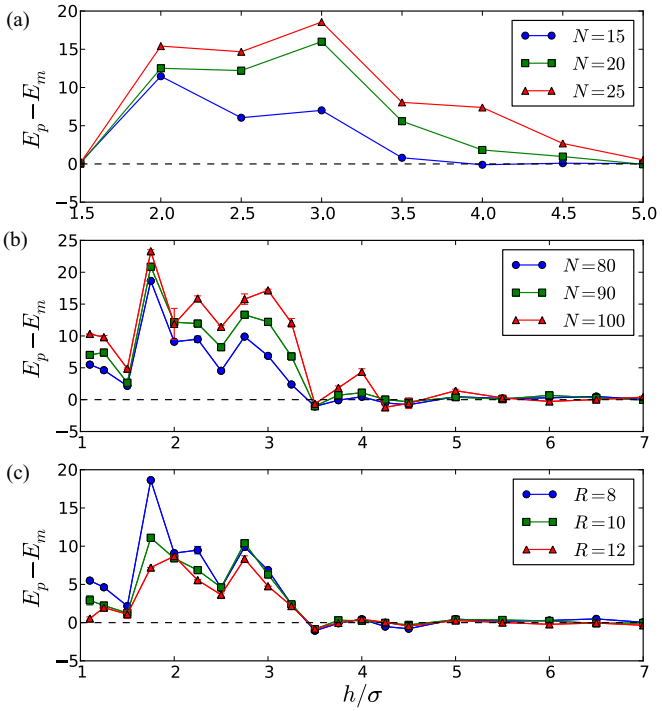

FIG. 3. (Color online) Dependence of average energy difference (in units of k_BT) between polar and midcell clusters, $E_p - E_m$, on (a) cluster size for 2D shells with $R = 8\sigma$, and for 3D shells where (b) N is varied with shell curvature fixed or (c) curvature is varied with N fixed. The number of particles or the size of the outer radius is shown in the legends. (Error bars were estimated by halving the data and calculating the fluctuation in $E_p - E_m$.)

In Fig. 3 we plot the energy difference between the poles and midcell as a function of shell thicknesses. For clusters in 2D shells, polar clusters always have greater energy [see Fig. 3(a)] due to being bent, and this energy difference increase with N. This energy difference goes away in thicker shells as the cluster becomes circular. This also occurs in 3D shells, and at large values of $h/\sigma > 5$ the energy difference vanishes as the cluster is spherical regardless of whether it is at the pole or midcell. For very thin shells ($h/\sigma < 1.5$) the cluster is a 2D sheet consisting of a single layer of particles, and the energy difference is greater than zero as the sheet has additional bending energy at the pole. At intermediate h/σ, the cluster is neither a 2D sheet nor spherical, and its energy at the pole is always greater than at midcell. The largest energy difference happens when a cluster goes from one layer thick to two. When

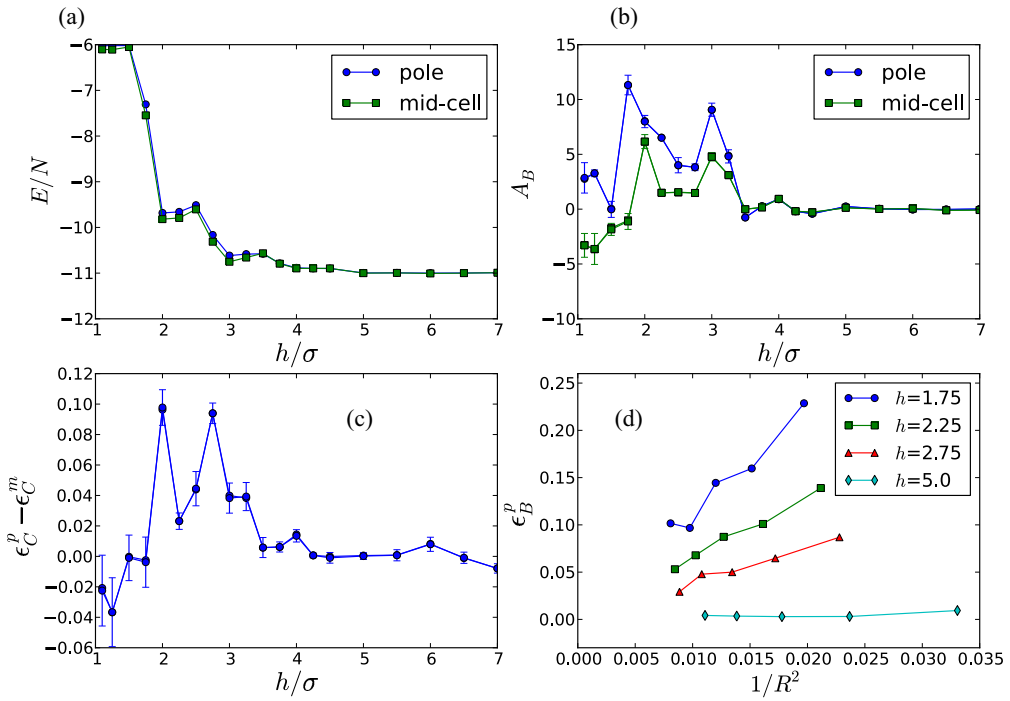

FIG. 4. (Color online) Energetics (all energy is in units of k_BT) of polar and midcell clusters with $N = 90$. (a) Energy per particle of polar and midcell clusters versus shell thickness in a shell with $R = 8\sigma$. (b) Fitted bending energy cost, A_B (in units of k_BT/σ^2) for polar and midcell clusters versus shell thickness. (c) Difference in fitted cluster energy per particle, ϵ_C, between pole and midcell versus shell thickness. Error bars on fitted parameters shown in (b) and (c) were determined using the bootstrap method. (d) The dependence of bending energy per particle, ϵ_B as a function of $1/R^2$ (in units of $1/\sigma^2$) at different shell thicknesses.

$h/\sigma \approx 2$ the cluster is able to form a regular hexagonal close packed arrangement midcell [see Fig. 1(b) as an example], but is frustrated at the poles. As h/σ increases this frustration decreases and allows the polar cluster to pack better, reducing the energy difference. The same phenomenon happens again when the cluster transitions from two to three layers at $h/\sigma \approx 3$. Interestingly at $h/\sigma \approx 3.5$ and $h/\sigma \approx 4.5$ our simulations show that polar clusters actually have lower binding energy on average than those at midcell. Not surprisingly, as N increases [Fig. 3(b)], the energy difference increases. Figure 3(c) shows the effect of curvature on the energy difference. For nonspherical clusters ($h/\sigma < 3$), increasing the outer radius lowers the energy difference since a portion of the energy difference arises from bending whose energy goes down with decreasing curvature.

We now explore the cluster energetics of the 3D clusters in greater detail and try to determine what factors play a potential role as both the shell thickness and curvature are changed. Since the energy of a cluster is an extensive quantity, we show in Fig. 4(a) the total binding energy at both the pole and midcell normalized by N. Now the previously described transitions can be seen more clearly as the cluster changes from one layer to two, and from two layers to three, etc. We consider that the energy of a cluster at either $\mu = \{p,m\}$, can be written as $E^\mu/N = \epsilon_C^\mu + \epsilon_B^\mu$ where ϵ_C^μ and ϵ_B^μ are, respectively, the packing and bending energy per particle. The packing energy will depend on h and potentially on R and in principle could be different between the pole and midcell due to defects that may be different between the two locations. The bending energy, ϵ_B^μ, depends on both h and R and will be different between midcell and the poles. At fixed shell thickness h, this bending energy should go as $\epsilon_B^\mu = A_B^\mu/\bar{R}^2$ where $\bar{R} = (R - h/2)$ is the mean radius of curvature of the cluster and A_B^μ is a proportionality constant that gives the bending energy cost. At each h we fit $E/N = \epsilon_C + A_B/\bar{R}^2$ versus $\bar{R}$ for both polar and midcell clusters. The resulting bending energy cost, A_B at different values of h/σ for both polar and midcell clusters is shown in Fig. 4(b). At values of h/σ before the cluster transitions to being spherical, polar clusters always show a greater bending energy cost than do midcell clusters. This is to be expected as clusters at the pole are bent in two independent directions whereas those at midcell are only bent in one. Trends in this cost as the shell thickness increases are less clear. It is apparent that at near integer values of h/σ, the associated cost of bending is dramatically increased [see Fig. 4(b)]. In Fig. 4(d) we show the resulting bending energy per particle ϵ_B^p at the pole as a function of the shell radius at different values of the shell thickness. At large h, clusters are spherical, and so there is no associated bending energy due to the shell. However, for thinner shells, the linear dependence of the bending energy versus $1/\bar{R}^2$ can be seen.

With respect to the cluster energy associated with packing, ϵ_C^μ, we plot the energy difference between the pole and midcell from the fitted values [Fig. 4(c)]. Interestingly, at the intermediate values of h/σ, the polar clusters are always less well packed and hence have a greater energy than those at midcell [see Figs. 1(b) and 1(c)] for an example of the existence of additional defects in the polar regions compared to midcell). As shown below, at certain h/σ this can lead to greater structural entropy at the poles and, hence,

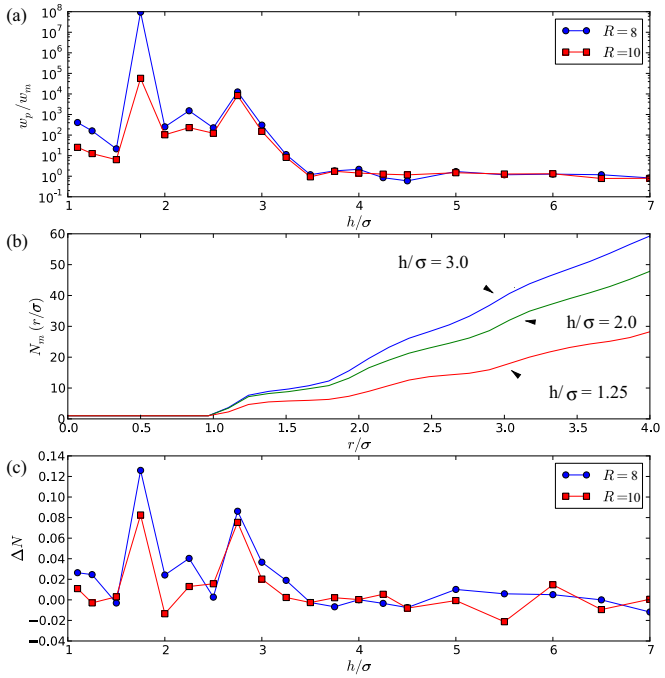

FIG. 5. (Color online) (a) Ratio of the number of cluster configurations at the pole to midcell w_p/w_m as a function of shell thickness, h/σ. (b) The average number of particles in a cluster, $N_\mu(r/\sigma)$ within a fixed-size sphere with radius r/σ at different shell thicknesses (here $\mu = m$, midcell). (c) The average difference in the number of nearest neighbors ΔN between midcell and polar clusters. Positive ΔN correspond to midcell clusters having on average a higher number of nearest neighbors and is a measure of the number of defects that exist within the polar cluster. In all figures, the cluster size was $N = 80$ and $R = 8\sigma$ unless otherwise specified.

potentially a lower free energy which would favor polar localization.

The last term in Eq. (2), w_p/w_m, is due to the configurational entropy difference between the pole and the midcell. The entropy of the cluster, S^μ, is associated with number of configurations that have the same energy E^μ. For all h/σ that cause the cluster to be non-spherical, Fig. 3 shows that the energy of clusters at the pole is always greater than at midcell in two and three dimensions. For clusters in two dimensions this always led to localization being favored at midcell. However, for clusters in 3D shells, localization could occur at the poles ($f_p/f_m > 1$) at certain values of h/σ. Hence for these h/σ, the entropy of the cluster at the pole must be significantly greater than that at midcell leading to the polar cluster having a lower free energy. In Fig. 5(a) we show the calculated w_p/w_m [using Eq. (2)] as a function of h/σ for different shell curvatures. We now show how this entropy difference arises from defects.

From our simulations, we find that non-spherical clusters at midcell form well-packed configurations [see Fig. 1(b)], whereas polar clusters are less well packed and possess additional defects [see Fig. 1(c)]. Ideally, clusters pack into a hexagonal close packed structure, where within a layer, a particle has six nearest neighbors, and depending on whether it resides in the interior or on the surface, may have six or three additional nearest neighbors respectively. Most particles show the ideal packing arrangement [see Fig. 1(b)], but some reside near defects which serve to reduce their coordination number [see circles in Fig. 1(c)]. To assess how well packed clusters are in a particular region, we look at the average number of particles $N_\mu(r/\sigma)$, that fall within a sphere of radius, r/σ, around each particle. (We find this by averaging over all particles in a cluster, and over all clusters in a particular region, μ). In Fig. 5(b) we show the average number of particles as a function of radial distance for midcell clusters of differing shell thicknesses. The distributions show steplike increases as one passes through the nearest neighbor shell and then the next nearest neighbor shell and so on. Semispherical clusters ($h/\sigma > 2.0$) have ≈ 9 nearest neighbors at $r/\sigma 1.1$, whereas single-layer clusters ($h/\sigma = 1.25$) have ≈ 6. We find that polar clusters consistently have a smaller average number of nearest neighbors than midcell clusters arising from the presence of defects in the polar cluster [compare Fig. 1(b) and 1(c)]. We characterize the number of defects, ΔN, by taking the difference $\Delta N = N_m(r/\sigma) - N_p(r/\sigma)$ at $r/\sigma = 1.1$. This is shown in Fig. 5(c) as a function of shell thickness. The greater the ΔN, the more defects there are at the pole, each of which can take various positions within the polar cluster. This results in the polar cluster having greater entropy. Indeed, we find a high correlation between ΔN and w_p/w_m.

V. DISCUSSION

We have shown that a cluster confined within a spherocylindrical shell can be localized to either the pole or midcell, depending on the shell's thickness. The selective pressure results from a competition between bending energy cost and the entropic gain associated with defects. For clusters in 2D shells, the additional bending energy of a cluster at a pole always favored localization midcell. However, in 3D shells, the interplay between the cluster's energy and entropy became more complex and led to the possibility of localizing to either region. We showed that the additional entropy at the pole was related to the presence of additional defects in polar clusters compared to midcell. At certain shell thicknesses, this additional entropy could give polar clusters an overall lower free energy, favoring localization there.

Our simulations were motivated by recent cell biology experiments showing the localization of molecules within the periplasmic space of certain bacteria. In order to relate our findings to bacterial geometries, we note that bacteria have diameters around 1 μm, and in our simulations we used $D = 8\sigma$ to 12σ, which would correspond to particle diameters of $\sigma \approx 80$–100 nm. This is clearly much bigger than the periplasmic space, which is around 20 nm in thickness, but could be comparable to the space between the nucleoid and the inner membrane. Nevertheless, we did find that as the particle number was increased, confinement effects extended to larger thicknesses, and so we would predict that if we could simulate much larger systems of particles similar trends would be seen. Indeed, for the localization of small dye molecules in the periplasm whose clusters consist of several layers, the clusters grow to sufficient size where they become nonspherical and confinement effects as identified here could still play a role.

Kinetic effects may also be important in the localization of biomolecular clusters in cellular systems. We have found that clusters at the pole tend to have smaller diffusion coefficients

on average than those at midcell (data not shown). If we consider that most biomolecular clusters grow throughout a cell's life cycle, these differences in diffusion between pole and midcell could favor the cluster being trapped at the pole. We are currently exploring this topic further. Studying the localization of clusters in confining shells such as presented here could be tested experimentally using suspended colloids in confining microfluidic channels to potentially examining the localization of molecules in bacteria that have periplasmic spaces of differing thickness. Further experiments are needed to determine the relevance of the competition between entropy and energy identified in this work for localizing clusters within real systems.

ACKNOWLEDGMENTS

E.E. would like to acknowledge the support of Natural Sciences and Engineering Research Council of Canada (NSERC) in carrying out this research.

[1] S. Thiem, D. Kentner, and V. Sourjik, EMBO J. **26**, 1615 (2007).
[2] D. Greenfield, A. L. McEvoy, H. Shroff, G. E. Crooks, N. S. Wingreen, E. Betzig, and J. Liphardt, PLoS Biol. **7**, e1000137 (2009).
[3] A. B. Lindner, R. Madden, A. Demarez, E. J. Stewart, and F. Taddei, Proc. Natl. Acad. Sci. U.S.A. **105**, 3076 (2008).
[4] G. R. Bowman, L. R. Comolli, J. Zhu, M. Eckart, M. Koenig, K. H. Downing, W. Moerner, T. Earnest, and L. Shapiro, Cell **134**, 945 (2008).
[5] G. Ebersbach, A. Briegel, G. J. Jensen, and C. Jacobs-Wagner, Cell **134**, 956 (2008).
[6] E. Maisonneuve, L. Fraysse, D. Moinier, and S. Dukan, J. Bacteriol. **190**, 887 (2008).
[7] J. Winkler, A. Seybert, L. König, S. Pruggnaller, U. Haselmann, V. Sourjik, M. Weiss, A. S. Frangakis, A. Mogk, and B. Bukau, EMBO J. **29**, 910 (2010).
[8] B. R. Parry, I. V. Surovtsev, M. T. Cabeen, C. S. O'Hern, E. R. Dufresne, and C. Jacobs-Wagner, Cell **156**, 183 (2014).
[9] H. Wang, N. S. Wingreen, and R. Mukhopadhyay, Phys. Rev. Lett. **101**, 218101 (2008).
[10] S. Saberi and E. Emberly, PLoS Comp. Biol. **6**, e1000986 (2010).
[11] S. Saberi and E. Emberly, PloS ONE **8**, e64075 (2013).
[12] A.-S. Coquel, J.-P. Jacob, M. Primet, A. Demarez, M. Dimiccoli, T. Julou, L. Moisan, A. B. Lindner, and H. Berry, PLoS Comp. Biol. **9**, e1003038 (2013).
[13] L. Ping, D. A. I. Mavridou, E. Emberly, M. Westermann, and S. J. Ferguson, PloS ONE **7**, e38427 (2012).
[14] P. N. Segrè, E. Herbolzheimer, and P. M. Chaikin, Phys. Rev. Lett. **79**, 2574 (1997).
[15] B. Lin, J. Yu, and S. A. Rice, Phys. Rev. E **62**, 3909 (2000).
[16] E. R. Dufresne, D. Altman, and D. G. Grier, Europhys. Lett. **53**, 264 (2001).
[17] B. Cui, H. Diamant, and B. Lin, Phys. Rev. Lett. **89**, 188302 (2002).
[18] C. Lutz, M. Kollmann, and C. Bechinger, Phys. Rev. Lett. **93**, 026001 (2004).
[19] C. R. Nugent, K. V. Edmond, H. N. Patel, and E. R. Weeks, Phys. Rev. Lett. **99**, 025702 (2007).
[20] G. Perkins and R. Jones, Physica A **189**, 447 (1992).
[21] T. M. Squires and M. P. Brenner, Phys. Rev. Lett. **85**, 4976 (2000).
[22] Y. Saito, M. Dufay, and O. Pierre-Louis, Phys. Rev. Lett. **108**, 245504 (2012).
[23] S. M. Anthony, M. Kim, and S. Granick, J Chem. Phys. **129**, 244701 (2008).
[24] W. H. Press, S. A. Teukolsky, W. T. Vetterling, and B. P. Flannery, *Numerical Recipes* (Cambridge University Press, New York, NY, 1992).